DOI: 10.61782/fa.2025.0197

FORUM ACUSTICUM
EURONOISE 2025

CHARACTERIZATION OF THE ACOUSTIC BEHAVIOR OF RAW EARTH COATINGS

Mathias Ziapkoff[1*] **Philippe Glé**[1] **Arthur Hellouin de Menibus**[2]
Thibaut Blinet[3] **Catherine Guigou Carter**[3]
[1] UMRAE, CEREMA, Univ Gustave Eiffel, IFSTTAR, Strasbourg, France
[2] Matélow, Rennes, France
[3] Centre Scientifique et Technique du Bâtiment, Grenoble / Marne la Vallée, France

ABSTRACT

Raw earth systems are gaining increasing interest in civil engineering due to their low energy and carbon impact, particularly raw earth coatings, which are still underexplored compared to other types of coatings such as those using lime or cement. The objective of this article, which is part of the CarAc'Terre project, is to characterize the behavior of these coatings in terms of acoustic dissipation. The aim is to analyze whether these materials behave in a purely elastic manner or if visco-thermal phenomena need to be taken into account. Experiments have been conducted at material scale on different coatings prepared by masons, with different earths and fiber contents. Acoustical properties were determined with a Kundt Tube in normal incidence and resistivity, porosity, and elasticity of the materials were also measured. These results were then compared with specific models based on theoretical approaches. The analyses revealed that raw earth coatings exhibit complex behaviors that may require consideration of both elastic and visco-thermal dissipation mechanisms. This study contributes to a deeper understanding of the acoustic properties of these materials, opening up new avenues to model the acoustic behavior of a wide variability in earth coating formulation.

Keywords: *Acoustics, Raw earth coatings, Resistivity, Porosity, Elasticity*

**Corresponding author*: *mathias.ziapkoff@cerema.fr.*

1. INTRODUCTION

The building sector is currently facing two major challenges: promoting the well-being of occupants [1] while minimizing the environmental impact of the materials and technical solutions used, which account for 40% of global energy consumption [2]. The use of sustainable materials, such as biosourced or geosourced materials, characterized by high thermal and acoustic performance, is an ideal solution in this context [3–5]. Among these materials, there is growing interest in raw earth systems, particularly hemp-earth concretes commonly referred to as "light earth".

Unlike other traditional hemp concretes, light earth concretes are biosourced granular materials produced by mixing hemp particles with clay. They can be used for construction work using formwork, projection, or block casting techniques, with or without wood. The use of a clay binder offers several advantages, including a carbon footprint around five times lower than that of hemp-lime, as the hardening of clay is reversible, unlike that of lime and cement. The hemp concrete family is valued both for its hygrothermal properties [6–9] and, as porous media, for their acoustic properties, which are crucial for guaranteeing a high level of safety and quality of life for inhabitants [10–13]. These studies have led to a better understanding of acoustic dissipation mechanisms within the material and have tested the applicability of traditional acoustic models such as Biot's poro-elastic approach [14] or the JCAL (Johnson-Champoux-Allard-Lafarge) model [15, 16].

However, analyzing the acoustic properties of light earth is not enough, as this material is rarely used alone at the wall or building scale by craftsmen. Indeed, it is com-

mon practice to add one or more layers of coating, a mixture of binder and additives (fibers, sand, aggregates) that provide better resistance but strongly limit sound absorption [13, 17]. Traditional lime or cement-based coatings are well known but are being questioned for their environmental impact. Raw earth coatings, on the other hand, although less studied, seem promising and are increasingly being considered [13,17–20]. However, there is still a lack of knowledge about the influence of coating formulation, such as its thickness or the nature of the binder employed.

The aim of this article, which is part of the CarAc'Terre project, is to characterize the acoustic behavior of different raw earth coating formulations applied to a layer of light earth, with a view to assessing the influence of formulation and initiating relevant numerical modeling. The aim is to determine whether the coating behaves purely elastically or whether visco-thermal phenomena need to be taken into account. This work is structured in three sections. The first section presents the study materials with the different coating formulations, as well as the experimental procedure for determining their acoustic and mechanical properties. Next, the first experimental results are analyzed, and initial trends are identified. Finally, the measurements are compared with numerical modeling proposals, considering the behavior of the two layers as purely isotropic elastic, as a porous-rigid, or as poro-elastic.

2. MATERIALS AND METHODS

2.1 Materials description

2.1.1 Raw materials

In the case of the light earth (i.e. "l-e"), the hemp particles are processed by the Planète Chanvre association, whose plant is located in Aulnoy (77). The earth used is betonite clay extracted from a single deposit in the commune of Le Buisson de Cadouin (24) and processed in the plant located in the commune of Mazeyrolles (24) by the Lafaure company.

For the coatings, two types of sifted re-employed clay, "Sygogne" and "Paix," were supplied by Totem Terre et Couleur, based in Saint-Gonlay (35). Two varieties of sand were also incorporated: 0/4 sand or 0/2 sand obtained from manual sieving of 0/4 sand using a 2,25 mesh sieve. Finally, four types of biosourced fibers were considered. Short-staple hemp wool was sourced from Agrochanvre (50), flax shiv from the Bosc Nouvel textile flax mill (76), Isocanna-type hemp shiv from Saint-Astier (24), and chopped straw fibers from a farm in Saint-Maden (94).

2.1.2 Samples manufacturing

The samples were made by Arthur Hellouin de Menibus from Matelow (35), a company specializing in light earth construction and training for professionals, Julia Cahour, Morgane Geffroy, Alice Lamy and Andra Varouchas. Moulds with a diameter of $100mm$ and different heights were prepared to form the samples into cylindrical shapes, while leaving a reserve of varying thickness for the coating. A total of 23 coating formulations were applied to the same light earth base. The light earth was applied with low compaction to avoid springback and guarantee a theoretical wet thickness of $30mm$. Four samples per formulation were prepared at the same time with three coatings and one uncoated as shown in Fig. 1.

Figure 1: Formulation example with three coated samples (A, C, D) and one uncoated sample (B).

Each formulation differs in terms of coating thickness, type of sand used, presence or absence of biosourced fibers, type of fibers, and finishes (trowel, sponge) during manufacture. To describe the formulation proposed, the samples are named according to a common nomenclature, $T\_F\_f\_e\_X$ or $T\_S\_f\_e\_X$, presented in Tab. 1. The dosages were carried out in proportion by volume, and the constituents were weighed each time to find the corresponding mass dosage.

Table 1: Sample nomenclature.

Symbol	Definition		Acronym
T	Type of earth	Earth "la Sygogne"	T1
		Earth "la Paix"	T2
F	Type of fiber	Short-staple hemp wool	L
		Flax shiv	A
		Hemp shiv	C
		Chopped straw fibers	P
		Lower fiber content used	min
S	Type of sand	0/2 sand	S02
		0/4 sand	S04
f	Type of finition	None	
		Trowelled surface	Tal
		Trowelled and sponged surface	TalEp
e	Thickness	$1mm$ thickness	1
		$2mm$ thickness	2
		$3mm$ thickness	3
		$2mm$ thickness	4
		$6mm$ thickness	6
		$10mm$ thickness	10
X	Sample index	N°1	A
		N°2	B
		N°3	C
		N°4	D

It is important to note that during the application of the coating, a certain amount of it penetrated into the microstructure of the light earth. Therefore, for the remainder of this work, it was necessary to estimate the actual thickness of the coating $e_{coating}$, presented in Tab. 2, from the coating density $\rho_{coating}$, the total mass of the sample m_{tot} and the mass of the light earth m_{l-e}. Considering a final coating volume that is always cylindrical, with R being the radius of the cylinder, we deduce $e_{coating}$ with Eqn. (1) below:

$$e_{coating} = \frac{\frac{m_{tot} - m_{l-e}}{\rho_{coating}}}{\pi R^2} \quad (1)$$

According to the results in Tab. 2 and the calculation of the relative deviation Δe between the theoretical and real coating thicknesses, the higher the theoretical coating thickness, the lower the relative deviation. This implies a lesser influence of its penetration into the microstructure of the light earth.

The samples were then stored at room temperature ($15 - 20°C$) and transported to the laboratory where they were weighed, their dimensions recorded, and then dried in an oven for 12 days at $50°C$ with a relative humidity maintained at 20% (Fig. 2a). Once this operation was complete, they were stored for a stabilization phase under the same conditions as in the experimental chamber ($\approx 20°C$, 50% RH) for at least 24 hours before the first tests (Fig. 2b). Once stabilized, the samples were weighed again and their dimensions were recorded to assess the absence of shrinkage after conditioning. The average thickness of the uncoated samples measured at $28,6mm$ with a coefficient of variation of 2% and an average density of $319kg/m^3$ with a coefficient of variation of 3% show that these samples can be considered comparable.

(a) (b)

Figure 2: Oven drying (a) and laboratory stabilisation (b) of the samples.

Table 2: General characteristics of coatings.

Nomenclature	$e_{theorical}$ (mm)	e_{real} (mm)	Δe (%)	$\rho\ (kg/m^3)$
$T1\_L\_1$	1	3,9	288	1369
$T1\_L\_2$	2	4,8	138	
$T1\_L\_3$	3	6,6	119	
$T1\_L\_4$	4	6,6	64	
$T1\_L\_6$	6	9,1	52	
$T1\_L\_10$	10	11,1	16	
$T1\_S02\_1$	1	3,6	259	2020
$T1\_S02\_2$	2	3,7	86	
$T1\_S02\_3$	3	4,2	39	
$T1\_S02\_4$	4	5,1	27	
$T1\_S02\_6$	6	7,1	18	
$T1\_S02\_10$	10	10,4	4	
$T1\_S04\_10$	10	11,5	15	1978
$T2\_S04\_10$	10	10,8	8	1977
$T1\_A\_6$	6	7,4	23	1473
$T1\_A\_10$	10	11,7	17	
$T1\_A\_min\_6$	6	7,9	31	1802
$T1\_A\_min\_10$	10	11,6	16	
$T2\_A\_10$	10	11,9	19	1423
$T1\_P\_10$	10	11,5	15	1606
$T1\_C\_10$	10	11,0	10	1375
$T1\_C\_Tal\_10$	10	10,6	6	
$T1\_C\_TalEp\_10$	10	10,4	4	

2.2 Experimental methods

2.2.1 *Kundt Tube*

Two main properties characterize the acoustic behavior of our samples at the material scale: insulation, represented by the transmission loss TL (dB), and acoustic correction, characterized by the absorption coefficient α $(-)$. In this work, we consider only the airborne transmission mode, thus not taking into account the so-called solid-borne noise.

The characterization methods used in this work are based on the use of a or Kundt Tube, shown in Fig. 3, at normal incidence. The same device can be used to determine sound absorption, the sound transmission loss, and the intrinsic properties of the material. To obtain the absorption coefficient, the three-position method without a cavity is used, while the transmission loss and intrinsic properties are measured by inducing an 18 mm plenum to free up the rear face of the samples. These two methods are presented in the thesis work of Philippe Glé [13].

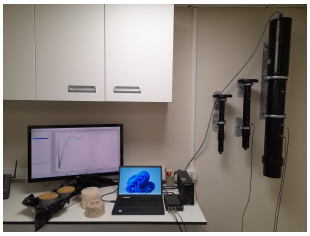

Figure 3: Kundt Tubes of different diameters and measurement acquisition device.

As mentioned in the introduction, taking inspiration from the work of Glé *et al.* [21] we can consider the two layers (light earth and coating) as having purely elastic behavior, with a rigid or poro-elastic skeleton. In the case of a purely elastic material, considered here as isotropic, only the mechanical contributions come into play. They are described by the density ρ, the Young's modulus E, the Poisson's ratio ν and the damping factor η, and can be identified using specific tests. The assumption of a rigid skeleton, considering only the porous phase of the material, is based on acoustic dissipations derived solely from visco-inertial and thermal effects. Advanced acoustic models such as the JCAL model characterize the porous behavior of a material based on six main parameters: porosity ϕ, resistivity σ, tortuosity α_∞, viscous and thermal characteristic lengths Λ and Λ', and static thermal permeability Θ_0. From these parameters, it is possible to derive the sound transmission loss and the sound absorption coefficient. It is generally common to determine the first three parameters (ϕ, σ, and α_∞) directly with experimental devices and to estimate the last three indirectly because they are more difficult to measure. When indirect estimation is also impossible, it is customary to simplify acoustic models, as we shall see in the last section. Finally, poro-elastic behavior combines the three dissipative effects based on the work of Biot [14, 22].

2.2.2 *Porosity*

Porosity ϕ $(\%)$, commonly considered to be open porosity in acoustics, is determined using the air volume comparison method mentioned by Leclaire *et al.* [23], illustrated in Fig. 4a. Conventional porosity measurements are used to characterize the porosity accessible to air. However, in the case of light earth, multi-scale behavior is also based on intra-particle porosity (Olny and Boutin [24]). In this case, an indirect assessment of porosity is required. Porosity can be estimated either from the asymptotic low or high-frequency limits of the dynamic incompressibility modulus, or from the low-frequency limit of the surface impedance. Where this is not possible, porosity can be inverted using a model such as Zwikker-Kosten [25].

2.2.3 *Resistivity*

The resistivity, denoted σ (Pas/m^2), can be measured directly using a resistivity device (Fig. 4b) as explained in [13]. Resistivity can also be characterized indirectly in a Kundt Tube under the same conditions as absorption and the transmission loss at normal incidence, as described by Jaouen et al. [26]. We refer the reader to Philippe Glé's thesis [13] for more information on direct or indirect estimation methods for other acoustic parameters. In the remainder of this study, we will prioritize data obtained directly, but in cases where it is impossible to obtain such data, we will use indirect estimates.

(a) (b)

Figure 4: Porosity (a) and resistivity (b) devices.

2.2.4 *Mechanical properties*

The apparent density ρ of a porous material can be measured directly by estimating its mass and volume. This work, presented in Tab. 2, was carried out for coatings by Catherine Guigou Carter and Thibaut Blinet at CSTB, a partner in the project, using bars with dimensions of $284mm \times 24mm \times 24mm$. They also estimated the Young's modulus E and the damping factor η of the coatings, according to the NF EN 14146 standard [27]. The density of the light earth was averaged at Cerema over all 23 uncoated sample measurements. The other parameters are taken from the work of Glé *et al.* [21] or the LOB+HIE project [18], pending future tests at the laboratory's quasistatic mechanical analyzer (QMA).

3. RESULTS

3.1 Experimental results : Influence of thickness

During this test campaign, 23 raw earth coating formulations were tested to observe the influence of the multiple factors mentioned above. In this article, we focus on the influence of coatings thickness with the study on $T1\_L$ mixes (n°1 to 5), corresponding to coating thicknesses of 1, 2, 3, 4, and 6 mm. The mean data for the three coated samples, for each thickness, are plotted with their standard deviations as uncertainty bars in Fig. 5a and Fig. 5b.

Fig. 5a shows that the absorption coefficient decreases with increasing thickness. This observation can be explained by the fact that it is easier for the acoustic wave to penetrate the layer of light earth when the thickness of the coating is low. Because of its microstructure, the light earth layer allows more acoustic dissipation within the material, which increases acoustic absorption. However, according to Fig. 5b, and contrary to the absorption coefficient, as the thickness of the coating increases, so does the acoustic insulation of the sample. This finding, shared by [21], suggests that sound attenuation is not solely due to a mechanical contribution but involves other effects, such as viscous and thermal dissipation. Finally, we generally observe a stabilization of performance from a thickness of $4mm$.

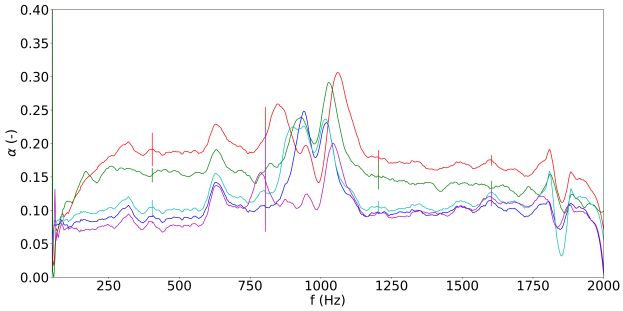

(a)

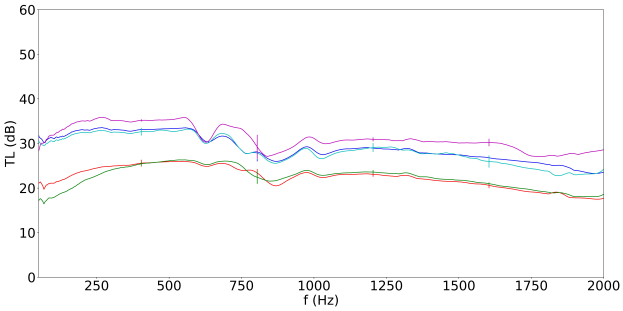

(b)

Figure 5: Evolution of the absorption coefficient $\alpha\ (-)$ (a) and the transmission loss $TL\ (dB)$ (b) as a function of frequency $f\ (Hz)$ for a $T1\_L$ sample of coating thickness $1mm$ (—), $2mm$ (—), $3mm$ (—), $4mm$ (—) or $6mm$ (—).

3.2 Numerical modeling

In this final section, we propose to model the acoustic behavior of one material using AlphaCell© software. We have chosen the $T1\_L\_10\_D$ sample, which has the advantage of having a theoretical coating layer $10mm$ thick, meaning its penetration into the layer of light earth is less influential. It is also a formulation for which the porosity and resistivity have been determined directly.

We consider the behavior of the layers to be purely isotropic elastic, porous-rigid, or poro-elastic. As explained above, the mechanical properties of the two layers are derived from experimental measurements or from the literature. The modeling of the porous character of the light earth-layered layer is based on the thesis of [13], who suggests considering hemp concretes with the JCA models coupling those of Johnson et al. [15] and Zwikker-Kosten [25], and globally requiring four param-

eters: porosity ϕ, resistivity σ, tortuosity α_∞, and viscous characteristic length Λ. The resistivity could be determined directly, whereas, due to the double-porosity phenomenon present in the material, the acoustic porosity had to be estimated indirectly, as well as the tortuosity and the viscous characteristic length.

On the other hand, for the porous nature of the coating, two rigid skeleton approaches are considered. Here, we use reduced models for the coating due to the relatively high resistivities of these materials, with other parameters having a more limited impact in this case. The first approach considers the coating with a JCAL model reduced to two parameters following the hypothesis of a perforated material geometry, σ and ϕ, considering the tortuosity equal to 1 and simplifying the relationships of the viscous and thermal characteristic lengths as well as the thermal static permeability. These relationships are shown in Tab. 3, which summarizes the mechanical and acoustic parameters of the two layers modeled, where r_1 is the radius of the pores considered to be cylindrical and μ is the shear viscosity of air, equal to $1,8 \times 10^{-5} Pa.s$. The second approach considers the coating with the Boutin-Geindreau granular model [28], requiring only two parameters, ϕ and r_2, the aggregates radius considered to be spherical, from which all the other acoustic parameters are deduced as described in Tab. 3. Note the closeness of the experimental values to those of [18], whether for light earth with, for example, a density of $295 kg/m^3$ and a porosity rate of 69%, or for earth coating with a density of $1500 kg/m^3$ or a Young's modulus of $2850 MPa$.

Table 3: Mechanical and acoustic parameters of the modelled layers. Data from [18] and [21] are shown as $^{[a]}$ and $^{[b]}$.

Parameters	Light earth	$T1\_L\_10\_D$ sample	
	JZK Model	JCAL model reduced	Granular model
Thickness (mm)	27,3	12	
$\rho\ (kg/m^3)$	319	1369	
$E\ (MPa)$	$2^{[a]}$	1711	
$\nu\ (-)$	$0,1^{[a]}$	$0,2^{[a][b]}$	
$\eta\ (\%)$	$10^{[b]}$	3	
$\phi\ (\%)$	65	50	
$\sigma\ (Pa.s.m^2)$	1,6E+3	1,5E+6	
$\alpha_\infty\ (-)$	1,6E+3	1,5E+6	
$r_1\ (m)$	×	$r_1 = \sqrt{\frac{8\mu}{\phi\sigma}}$	×
$r_2\ (m)$	×	×	$r_2 = \sqrt{\frac{3\beta^2\mu}{\sigma\left(-1+\frac{2+3\beta^5}{\beta(3+2\beta^5)}\right)}}, \beta = (1-\phi)^{\frac{1}{3}}$
$\Lambda\ (m)$	2,6E-4	r_1	$\frac{4\phi\alpha_\infty}{9(1-\phi)} r_2$
$\Lambda'\ (m)$	×	r_1	$\frac{2\phi}{3(1-\phi)} r_2$
$\Theta_0\ (m^2)$	×	$\frac{\phi r_1^2}{8}$	$\frac{(5-9\beta+5\beta^3-\beta^6) r_2^2}{15(1-\beta^3)\beta^3}$

A total of five models are compared with the experimental absorption coefficient (Fig. 6a) and transmission loss (Fig. 6b).

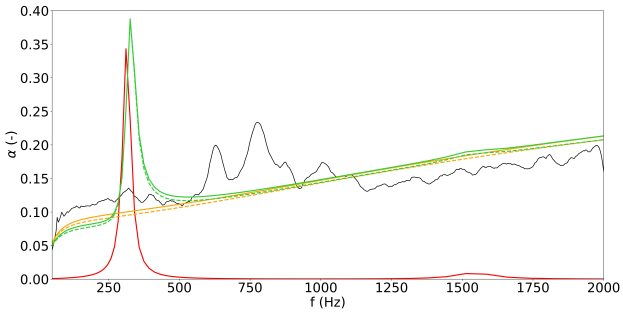

(a)

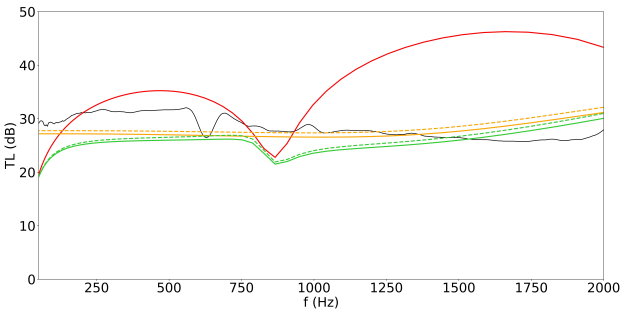

(b)

Figure 6: Comparison of the evolution of the absorption coefficient $\alpha\ (-)$ (a) and the transmission loss $TL\ (dB)$ (b) as a function of the frequency $f\ (Hz)$ for the coated sample $T1\_L\_10\_D$ between the experimental measurement (—), simulation of elastic bilayer behaviour (—), simulation of a porous-rigid bilayer behaviour using the reduced JCAL (—) or Boutin-Geindreau (- -) model and simulation of poro-elastic bilayer behaviour using the reduced JCAL (—) or Boutin-Geindreau (- -) model.

Analysis of Fig. 6a reveals that the assumption of purely elastic behavior of the two layers of the sample is insufficient to simulate its absorption behavior. On the other hand, the four other simulations, which take into account the porous character, seem to be closer to the experimental results. This suggests that the measured resistivity of the coating is fairly representative. The two categories of simulations have the advantage of being relatively simple, with few parameters, while providing a fairly relevant

prediction. This is particularly the case with poro-elastic behavior, which reproduces the resonance observed experimentally, although at lower frequencies. This resonance corresponds to that of the light eart layer, which is caused by the compression of its solid phase following acoustic stress. A second simulation later revealed that increasing the Young's modulus to $10MPa$ further improved the position of this resonance frequency. Finally, there was no major difference between the two approaches regarding the pore geometry of the coating.

The overall numerical prediction of the transmission loss by the five approaches is slightly poorer than that of the absorption coefficient, as shown in Fig. 6b. The hypothesis of purely elastic behavior of the sample should once again be ruled out, while the others seem to slightly underestimate the transmission loss at low frequencies and overestimate it at high frequencies. Overall, the simplified poro-elastic approach seems to be the most interesting, as it again reproduces the resonance of the lightened earth while providing a promising prediction regardless of the pore shape hypothesis.

4. CONCLUSION

This work, part of the CarAc'Terre project, focused on characterizing the acoustic behavior of different, as yet little-studied, raw earth coating formulations applied to light earth. We aimed to assess the influence of the formulation and propose an initial numerical modeling campaign for this two-layer material. After presenting the study materials with the different coating formulations, we described the methods for direct or indirect estimation of the acoustic and mechanical parameters required to characterize the acoustic performance of the samples. We then analyzed the initial experimental results, revealing the first trends. Among other things, it appeared that an increase in the thickness of the coating reduced the acoustic absorption of the bilayer, as opposed to the acoustic insulation. Finally, the measurements were compared with a proposal for numerical modeling, considering the behavior of the layers as purely elastic, porous-rigid, or poro-elastic. The poro-elastic approach appeared to be the most relevant, thanks to the simulation of mechanical and visco-thermal dissipation. This study raises a number of prospects for future work like improving the numerical approach by developing more accurate acoustic models or considering the scale of the wall and the entire building, which will be the subject of further studies as part of the project.

5. ACKNOWLEDGEMENTS

We would like to thank Julia Cahour, Morgane Geffroy, Alice Lamy and Andra Varouchas for their contribution to the coating samples. This project was funded by the French government as part of France Relance, now part of France 2030, and operated by ADEME.

6. REFERENCES

[1] S. Altomonte, J. Allen, P. M. Bluyssen, G. Brager, L. Heschong, A. Loder, S. Schiavon, J. A. Veitch, L. Wang, and P. Wargocki, "Ten questions concerning well-being in the built environment," *Building and Environment*, vol. 180, p. 106949, 2020.

[2] F. Pittau, F. Krause, G. Lumia, and G. Habert, "Fast-growing bio-based materials as an opportunity for storing carbon in exterior walls," *Building and Environment*, vol. 129, pp. 117–129, 2018.

[3] F. Asdrubali, "Green and sustainable porous materials for noise control in buildings: a state of the art," in *SAPEM-Symp. on the Acoustics of Poro-Elastic Materials*, 2011.

[4] N. H. Bhingare, S. Prakash, and V. S. Jatti, "A review on natural and waste material composite as acoustic material," *Polymer Testing*, vol. 80, p. 106142, 2019.

[5] M. Pedroso, J. de Brito, and J. Silvestre, "Characterization of eco-efficient acoustic insulation materials (traditional and innovative)," *Construction and Building Materials*, vol. 140, pp. 221–228, 2017.

[6] T. Colinart, T. Vinceslas, H. Lenormand, A. H. D. Menibus, E. Hamard, and T. Lecompte, "Hygrothermal properties of light-earth building materials," *Journal of Building Engineering*, vol. 29, pp. 2352–7102, 2020.

[7] F. Collet and S. Pretot, "Thermal conductivity of hemp concretes: Variation with formulation, density and water content," *Construction and Building Materials*, vol. 65, pp. 612–619, 2014.

[8] U. Dhakal, U. Berardi, M. Gorgolewski, and R. Richman, "Hygrothermal performance of hempcrete for ontario (canada) buildings," *Journal of Cleaner Production*, vol. 142, pp. 3655–3664, 2017.

[9] M. Sáez-Pérez, M. Brümmer, and J. Durán-Suárez, "A review of the factors affecting the properties and performance of hemp aggregate concretes," *Journal of Building Engineering*, vol. 31, pp. 2352–7102, 2020.

[10] M. Areias Trindade, *Propriétés mécaniques, thermiques et acoustiques d'un matériau a base de particules végétales: approche expérimentale et modélisation théorique*. Theses, Conservatoire national des arts et metiers - CNAM, 2005.

[11] P. Glé, E. Gourdon, and L. Arnaud, "Acoustical properties of materials made of vegetable particles with several scales of porosity," *Applied Acoustics*, vol. 72, pp. 249–259, 2011.

[12] P. Glé, E. Gourdon, and L. Arnaud, "Modelling of the acoustical properties of hemp particles," *Construction and Building Materials*, vol. 37, pp. 801–811, 2012.

[13] P. Glé, *Acoustique des matériaux du bâtiment à base de fibres et particules végétales-outils de caractérisation, modélisation et optimisation*. Theses, INSA de Lyon, 2013.

[14] M. A. Biot, "Theory of propagation of elastic waves in a fluid-saturated porous solid. i. low-frequency range," *The Journal of the Acoustical Society of America*, vol. 28, pp. 168–178, 1956.

[15] D. L. Johnson, J. Koplik, and R. Dashen, "Theory of dynamic permeability and tortuosity in fluid-saturated porous media," *Journal of fluid mechanics*, vol. 176, pp. 379–402, 1987.

[16] D. Lafarge, P. Lemarinier, J. F. Allard, and V. Tarnow, "Dynamic compressibility of air in porous structures at audible frequencies," *The Journal of the Acoustical Society of America*, vol. 102, pp. 1995–2006, 1997.

[17] O. Kinnane, A. Reilly, J. Grimes, S. Pavia, and R. Walker, "Acoustic absorption of hemp-lime construction," *Construction and Building Materials*, vol. 122, pp. 674–682, 2016.

[18] T. Blinet, T. Falwisanner, G. Philippe, C.-G. Catherine, K. Elias, and B. Farid, "Propriétés acoustiques des matériaux biosourcés," *Rapport final CSTB-Cerema-DHUP*, 2018.

[19] P. Glé, E. Gourdon, L. Arnaud, K.-V. Horoshenkov, and A. Khan, "The effect of particle shape and size distribution on the acoustical properties of mixtures of hemp particles," *The Journal of the Acoustical Society of America*, vol. 134, pp. 4698–4709, 2013.

[20] M. Miranda Santos, *La terre crue à l'épreuve des ambiances sonores: un dialogue entre la mesure physique et les expériences sensibles.* Theses, Universitat Politècnica de Catalunya, 2022.

[21] P. Glé, G. Massossa-Telo, A. Hellouin de Menibus, M. Degrave-Lemeurs, and E. Gourdon, "Characterization and modelling of the sound reduction of hemp-clay walls in buildings," *Journal of Building Engineering*, vol. 40, p. 102315, 2021.

[22] M. A. Biot, "Theory of propagation of elastic waves in a fluid-saturated porous solid. ii. higher frequency range," *The Journal of the Acoustical Society of America*, vol. 28, pp. 179–191, 1956.

[23] P. Leclaire, O. Umnova, K. V. Horoshenkov, and L. Maillet, "Porosity measurement by comparison of air volumes," *Review of Scientific Instruments*, vol. 73, pp. 1366–1370, 2003.

[24] X. Olny and C. Boutin, "Acoustic wave propagation in double porosity media," *The Journal of the Acoustical Society of America*, vol. 114, pp. 73–89, 2003.

[25] C. Zwikker and C. W. Kosten, *Sound absorbing materials*. New York: Elsevier, 1949.

[26] L. Jaouen, E. Gourdon, and P. Glé, "Estimation of all six parameters of johnson-champoux-allard-lafarge model for acoustical porous materials from impedance tube measurements," *The Journal of the Acoustical Society of America*, vol. 148, pp. 1998–200, 2020.

[27] Afnor Editions, "NF EN 14146 : Méthodes d'essai pour pierres naturelles - Détermination du module d'élasticité dynamique (par la mesure de la fréquence de résonance fondamentale)," 2004.

[28] C. Boutin and C. Geindreau, "Periodic homogenization and consistent estimates of transport parameters through sphere and polyhedron packings in the whole porosity range," *Physical Review E—Statistical, Nonlinear, and Soft Matter Physics*, vol. 82, p. 036313, 2010.